PCCP

PAPER

View Article Online
View Journal | View Issue

Cite this: *Phys. Chem. Chem. Phys.*, 2015, **17**, 6314

Correlating structure with non-linear optical properties in $x As_{40}Se_{60}\cdot(1-x)As_{40}S_{60}$ glasses

Emma R. Barney,*[a] Nabil S. Abdel-Moneim,[a] James J. Towey,[a] Jeremy Titman,[b] John E. McCarthy,[c] Henry T. Bookey,[c] Ajoy Kar,[c] David Furniss[a] and Angela B. Seddon[a]

Received 3rd December 2014,
Accepted 22nd January 2015

DOI: 10.1039/c4cp05599c

www.rsc.org/pccp

A series of $x As_{40}Se_{60}\cdot(100-x)As_{40}S_{60}$ glasses, where x = 0, 25, 33, 50, 67, 75 and 100 mol% $As_{40}Se_{60}$, has been studied using neutron and X-ray total scattering, Raman spectroscopy and ^{77}Se MAS-NMR. The results are presented with measurements of non-linear refractive indices, n_2, and densities. There is no evidence for the formation of homopolar bonds in these glasses, but neutron correlation functions suggest that there is a non-random distribution of sulfur and selenium atoms in sulfur-rich glasses. The average number of sulfur atoms at a distance of 3–4 Å from a selenium atom, n_{SeS}, deviates from a linear variation with x in glasses containing <50 mol% $As_{40}Se_{60}$; n_2 for these glasses also varies non-linearly with x. Importantly, a direct comparison of n_2 and n_{SeS} gives a linear correlation, suggesting that n_2 may be related to the distribution of chalcogen atoms in the glasses.

1. Introduction

The low phonon energies, and large non-linear optical responses, exhibited by chalcogenide glasses enable them to transmit, and interact with, a broad spectrum of mid-infrared (mid-IR) light. These properties, coupled with an ability to act as laser hosts *via* the incorporation of rare earth ions, make chalcogenide glasses ideal candidates for a range of mid-IR applications, including new bright mid-IR fibre laser sources.

The As–S–Se glass system is of particular interest because melts require only moderate cooling rates (air cooling) to form a glass and it has a wide glass forming domain. The range of glass formation is bounded by the binary glass forming ranges of x = 5–45 at% As in As_xS_{100-x}, 0–62 at% As in As_xSe_{100-x}, and 0–85 at% Se in S_xSe_{100-x}.[1,2] As–S–Se glasses show good thermal stability, with resistance to crystallisation during fibre-drawing, and non-linear refractive indices, n_2, $>100x$ that of silica.[3,4] The effect on glass properties caused by varying the relative amounts of As, Se and S is well documented, but less well understood. For example, reported physical property measurements of $x As_{40}Se_{60}\cdot(100-x)As_{40}S_{60}$ glasses indicate that density[3,5] and glass transition temperature, T_g,[3,5,6] vary linearly with x yet n_2, important for active optical applications, does not.[3,4] Understanding the relationship between composition, structure and macroscopic properties will facilitate the development of glass compositions that are designed and tailored for specific optical devices.

Previous structural studies of As–Se–S glasses have predominantly used spectroscopic techniques. However, these methods have limitations in the information they can yield. ^{77}Se Nuclear Magnetic Resonance (NMR) studies give averaged evidence for the local environment of selenium,[7,8] but sulfur and arsenic NMR are less informative as bonding information cannot be gained directly. Numerous Raman scattering studies[2,3,9–11] have identified the characteristic vibrations of As–S, As–Se, S–S and Se–Se. S–S bond vibrations oscillate at relatively high wave numbers, because both atoms in the bond are light, giving rise to a band in the Raman spectra at 440–500 cm^{-1}.[2,3,9–11] When sulfur is bonded to the heavier arsenic or selenium atoms, the bond vibrational frequency was reported to red-shift to ~270–420 cm^{-1} and when the heavier oscillators (As and Se) are directly bonded (As–As, As–Se and Se–Se), bands in the wave number range 220–270 cm^{-1} are observed. Attempts have been made to relate these Raman spectral features to glass structure. However, due to the similar masses of As and Se, deconvolution of contributions from As–S and Se–S at ~350 cm^{-1}, or As–As, Se–Se and As–Se at ~250 cm^{-1}, is difficult (see ref. 2 and 10 for examples). One study of As-poor glasses, where homopolar chalcogen–chalcogen (Ch–Ch) bonds are an integral part of the glass network, indicated that there is a preference for Se–Se bonds over those of S–S or S–Se, concluding that selenium chains, and $[AsS_3]$ units, are more favourable than $[AsSe_3]$ units and sulfur chains.[10] However, Raman spectra for pure selenium and pure sulfur showed that

[a] *Faculty of Engineering, University of Nottingham, University Park, Nottingham, NG7 2RD, UK. E-mail: Emma.Barney@nottingham.ac.uk*
[b] *School of Chemistry, University of Nottingham, University Park, Nottingham, NG7 2RD, UK*
[c] *Institute of Photonics and Quantum Sciences, School of Engineering and Physical Sciences, Heriot Watt University, Edinburgh EH14 4AS, UK*

Se–Se bonds have a greater oscillator strength than S–S bonds.[2] This results in a greater intensity of the Se peaks in the Raman spectrum, and casts doubt on the conclusions drawn in ref. 10. In conclusion, difficulties in quantitatively interpreting spectroscopic measurements, coupled with a lack of structural information beyond the direct bonds in the glass, limit the use of NMR and Raman in aiding the understanding of how chalcogen atoms are distributed in chalcogenide glasses.

In contrast to spectroscopic techniques, neutron and X-ray correlation functions, $T(r)$, yield quantitative measurements of glass structure. The results give information about the local environments of atoms in the glass, and how those structural units link together to form a 3-D glass network. Although there have been several total scattering studies[12–14] of the stoichiometric glasses, $As_{40}Se_{60}$ and $As_{40}S_{60}$, and of binary glasses with varying cation to anion ratios, $As_{1-x}Se_x$ and $As_{1-x}S_x$, there are fewer which study the effect of mixing S and Se chalcogen anions on the network structure. Furthermore, there is not much information on how glass structure underpins macroscopic glass properties.

The stoichiometric glass forming system, $x As_{40}Se_{60}\cdot(100-x)As_{40}S_{60}$ (where x = 0, 25, 33, 50, 67, 75, 100 mol%), has been chosen for this study to minimise the number of homopolar (As–As, Ch–Ch) bonds and simplify the structure.[13] Along this compositional tie line, an ideal glass would be solely constructed of [$AsCh_3$] units, with each chalcogen bonding to two arsenic atoms to provide the network connectivity. We compare structural insights gained from neutron and X-ray total scattering, supported by Raman and ^{77}Se NMR, with the nonlinear optical performance of chalcogenide glasses, in terms of the nonlinear refractive index, n_2.

2. Total scattering theory

2.1. $i(Q)$ and $T(r)$

A neutron diffraction experiment measures the differential cross-section, $\frac{d\sigma}{d\Omega}$, which is equivalent to the total scattering from the sample, $I^N(Q)$, where Q is the magnitude for the scattering vector for elastic scattering.[15] The total scattering is the sum of the self-scattering, $I^s(Q)$ (the interference between scattered waves from the same nucleus), and the distinct scattering, $i^N(Q)$ (the interference between scattered waves from different nuclei);

$$\frac{d\sigma}{d\Omega_n} = I^N(Q) = I^s(Q) + i^N(Q). \quad (1)$$

The Fourier transform of $i^N(Q)$ yields a real-space correlation function, $T^N(r)$. This is a measure of the frequency of the occurrence of interatomic distances in the sample and is calculated as:

$$T^N(r) = 4\pi\rho^0 r\left(\sum_i c_l \bar{b}_l\right)^2 + \frac{2}{\pi}\int_0^{Q_{max}} Q i^N(Q) M(Q)\sin(rQ)dQ \quad (2)$$

where $M(Q)$ is a modification function, such as the Lorch function,[16] used to reduce termination ripples in the Fourier transform and ρ^0 is the atomic number density. c_l is the atomic fraction and $\bar{b}_l$ is the coherent neutron scattering length (see Table 1) for element l. The resolution in real-space depends on the modification function and the maximum momentum transfer, Q_{max}, of the experimental data.

Table 1 The variation in scattering power of As, S and Se for neutrons and X-rays

Element	Neutron scattering length, b	X-ray form factor, $f(0)$
S	2.847	16
As	6.58	33
Se	7.97	34

In the case of X-ray diffraction, the scattering data has a form factor dependence. This is removed by normalising the data using the Krogh-Moe and Norman method[17,18] to yield the distinct scattering $I^X(Q)$. X-rays scatter from the electron cloud of an atom, resulting in a relatively broad 'electron–electron' correlation function. To remove this broadening and obtain a correlation function, $T^X(r)$, that has good resolution, a sharpened distinct scattering spectra, $i^X(Q)$, is required. This is obtained by dividing $I^X(Q)$ by $\langle f(Q)\rangle^2$ (where $\langle f(Q)\rangle$ is the mean X-ray form factor for the sample and is related to the atomic number, Z, of the elements involved).[19,20] This new function approximates scattering from point sources;

$$i^X(Q) = \frac{I^X(Q)}{\langle f(Q)\rangle^2} \quad (3)$$

The X-ray correlation function, $T^X(r)$, obtained from a Fourier transform of $i^X(Q)$ is given by:

$$T^X(r) = 4\pi\rho^0 r + \frac{2}{\pi}\int_0^{Q_{max}} Q i^X(Q) M(Q)\sin(rQ)dQ \quad (4)$$

Neglecting the effect of form factors on X-ray peak shapes in $T^X(r)$, the correlation functions, $T^N(r)$ and $T^X(r)$, are the weighted summations over all the pairwise combinations of elements in the sample, $t_{ll'}(r)$:

$$T^N(r) = \sum_{l,l'} c_l \bar{b}_l \bar{b}_{l'} t_{ll'}(r) \quad \text{and} \quad T^X(r) = \sum_{l,l'} \frac{c_l Z_l Z_{l'}}{\langle Z\rangle^2} t_{ll'}(r) \quad (5)$$

2.2. Extracting coordination numbers from $T^N(r)$

Each peak in the neutron correlation function, $T^N(r)$, arising from a particular pair of elements l and l′. The coordination number, $n_{ll'}$, can be calculated from the peak area, $A_{ll'}$, and the interatomic distance, $r_{ll'}$, given by the position of the peak and according to:

$$n_{ll'} = \frac{r_{ll'} A_{ll'}}{(2-\delta_{ll'}) c_l \bar{b}_l \bar{b}_{l'}} \quad (6)$$

where $\delta_{ll'}$ is the Kronecker delta and $c_l\bar{b}_l\bar{b}_{l'}$ is the coefficient for $t_{ll'}(r)$. If the coordination number for $n_{ll'}$ and $n_{l'1}$ have been calculated using the area and position of a feature in $T^N(r)$ with a defined distance range, then the coordination numbers for ll′ and l′l atom pairs are related by the following identity

$$n_{ll'}c_l = n_{l'l}c_{l'} \quad (7)$$

The first peak in the neutron correlation function, $T^N(r)$, for a glass network constructed solely of [$AsCh_3$] (Ch=S or Se) units, is comprised of directly bonded As–Ch distances. The second peak arises from the next nearest neighbours in the glass and can comprised of a mix of up to nine X···X distances (where ··· denotes a non-bonding distance between two atoms). The various contributions can be written as an expansion of eqn (5)

$$\begin{aligned} T^N(r) &= c_{As}\bar{b}_{As}{}^2 n_{AsAs} + c_{As}\bar{b}_{As}\bar{b}_{Se} n_{AsSe} + c_{As}\bar{b}_{As}\bar{b}_S n_{AsS} \\ &+ c_{Se}\bar{b}_{Se}{}^2 n_{SeSe} + c_{Se}\bar{b}_{Se}\bar{b}_{As} n_{SeAs} + c_{Se}\bar{b}_{Se}\bar{b}_S n_{SeS} \\ &+ c_S\bar{b}_S{}^2 n_{SS} + c_S\bar{b}_S\bar{b}_{As} n_{SAs} + c_S\bar{b}_S\bar{b}_{Se} n_{SSe} \end{aligned} \quad (8)$$

If there is a linear change in the glass structure with composition, then a weighted sum of the two end member glasses, $x As_{40}Se_{60}$ + $(100 - x)As_{40}S_{60}$, will give a good approximation for the As–Ch contribution to the first peak in the neutron correlation function, and the As···As and As···Ch correlations contributing to the second peak, for a glass with composition $x As_{40}Se_{60}\cdot(100 - x)As_{40}S_{60}$. However, the weighted sum will overestimate the contributions from Se···Se and S···S correlations because mixing, *i.e.* the presence of Se···S distances, is neglected.

The expected difference between an experimental $T^N(r)$ and a $T^N(r)$ predicted by a weighted sum of $As_{40}Se_{60}$ and $As_{40}S_{60}$ can be calculated by a consideration of the Ch···Ch contribution to the second peak in the experimental data. It can be shown, using eqn (6) and (8), that the expected area for a peak comprised of all the possible Ch···Ch combinations is related to the total number of chalcogen neighbours, n_{ChCh}:

$$r_{ChCh}A_{ChCh} = c_{Se}\bar{b}_{Se}{}^2 n_{SeSe} + c_S\bar{b}_S{}^2 n_{SS} + c_{Se}\bar{b}_{Se}\bar{b}_S n_{SeS} + c_S\bar{b}_S\bar{b}_{Se} n_{SSe} \quad (9)$$

If it is assumed that the number of chalcogen atoms at a distance $r + \delta r$ from an Se atom, n_{SeCh}, and a S atom, n_{SCh} is the same, then

$$n_{ChCh} = n_{SS} + n_{SSe} = n_{SeSe} + n_{SeS} \quad (10)$$

Rearranging these equations for n_{SS} and n_{SeS}, substituting the result into eqn (9) and simplifying the result using the relationship in eqn (7), the following equation can be derived:

$$r_{ChCh}A_{ChCh} = n_{ChCh}(c_{Se}\bar{b}_{Se}{}^2 + c_S\bar{b}_S{}^2) - c_{Se}n_{SeS}(\bar{b}_{Se} - \bar{b}_S)^2 \quad (11)$$

The first term in eqn (11) is the contribution to the Ch···Ch peak from the weighted sum of Se···Se and S···S contributions. The difference between the weighted sum, and the experimental data is given by the second term and yields a peak arising from Se···S correlations. Fitting this residual allows n_{SeS} to be calculated. If there is no preference for like (or unlike) chalcogen atoms to be in the same [$AsCh_3$] unit, then the Se–S coordination number depends on the fraction of chalcogens which are sulfur, so that $n_{SeS} = (1 - (x/100))n_{ChCh}$. In $As_{40}Se_{60}$ ($x = 100$), $n_{SeS} = 0$ because there are no sulfur atoms in the glass. However, for $As_{40}S_{59}Se$ ($\sim x = 0$), all the chalcogen next nearest neighbours to the single Se atom would be sulfur and n_{SeS} = n_{ChCh} (= n_{SS} in $As_{40}S_{60}$). The structure of crystalline $As_{40}S_{60}$ predicts that n_{SS} for the glass should be approximately 7.33. Deviations from a linear variation in n_{SeS} from ~7.33 to 0 with increasing x would only occur if:

(1) There is a significant difference between the experimental arsenic correlations and those predicted by the weighted sum of the end members.

(2) There was a preference for like anions to cluster together.

(3) The number of S atoms around Se differs from the number of Se atoms around S in the distance range of interest.

3. Experimental setup

3.1. Sample preparation

A series of glasses, $x As_{40}Se_{60}\cdot(100 - x)$ $As_{40}S_{60}$, where x = 0, 25, 33, 50, 67, 75 and 100 mol% $As_{40}Se_{60}$, was made using high purity As (99.99999%, Furukawa Electric Ltd.), Se and S (both 99.999%, Materion). As, and Se, were further purified by heating under vacuum (10^{-3} Pa) at 310 °C, and 270 °C, prior to batching (15–20 g samples), which was carried out inside a glove-box ($\leq$0.1 ppm O_2, $\leq$0.1 ppm H_2O; MBraun). The silica glass ampoules (<1.0 ppm OH, ID/OD = 10 mm/14 mm, MultiLab.) in which the glasses were batched and melted, had been air-baked (1000 °C for 6 hours) and vacuum baked (1000 °C for 6 hours at 10^{-3} Pa) prior to use. The ampoule was sealed under vacuum (~10^{-3} Pa), placed in a rocking furnace held statically, raised at 30 °C h^{-1} to 250 °C and held isothermally for 2 h to ensure the chalcogens had fully melted. The furnace was then programmed to rock (±30° to horizontal axis) as the ampoule was heated to ~650 °C (30 °C h^{-1}) before being held isothermally with rocking for 12 h to achieve homogenisation. The furnace was then placed statically vertical and cooled at 60 °C h^{-1} to ~570 °C. A final isothermal dwell of ~2 hours, to fine and refine the glass, was given before quenching the glass. The ampoules were quenched using a jet of nitrogen gas and subsequently annealed at T_g for 30 minutes, before cooling slowly to ambient, producing small glass rod samples.

Sample compositions were characterised using a PANalytical MiniPal4 to collect X-ray Fluorescence (XRF) spectra and Scanning Electron Microscopy, in back scattered mode, was used to collect Energy Dispersive X-ray (EDX) spectra. Density measurements were carried out using a Quantachrome Micropycnometer, with helium as the displacement gas. Measurements of the glass transition temperature were carried out using a Perkin Elmer DSC7 Differential Scanning Calorimeter with water circulating chillers and an argon gas flow at the rate of 20 ml min^{-1}. For each measurement an initial "conditioning" temperature run was carried out by heating, and then cooling, the glass through the glass transition temperature, using a ramp rate of 10 °C min^{-1} to ensure all glasses had the same thermal history. The sample was then heated again at 10 °C min^{-1} to determine T_g. The value for T_g was calculated using two different methods. The first method was to determine the point of maximum gradient, $T_{g,max}$, taken as the maximum point in the derivative of the data. The second method was to calculate an "onset temperature", $T_{g,onset}$, using the intersection of two tangents fitted to the baseline, and the point of

maximum gradient in the T_g feature. The first method gives a larger value for T_g than the second.

3.2. *Z*-scan measurements of n_2

A standard *Z*-scan setup[21] was used to measure the nonlinear optical absorption, β, and nonlinear refractive index, n_2, of the seven As–S–Se glasses. The laser system was a Spectra Physics optical parametric generator-optical parametric amplifier combination with a Ti:sapphire laser and regenerative amplifier. The laser pulse width was ~120 fs and the corresponding spectral width was 12 nm. The measurements were performed using a laser of wavelength 1550 nm, pulse repetition rate of 1 kHz and a beam waist of 35 μm. Open and closed (20% transmission) aperture scans were recorded simultaneously to measure the nonlinear coefficients. The samples were prepared by cutting a 10 mm diameter discs from the as-annealed glass rods. Both surfaces of the discs were polished to a 1 μm finish. To ensure the surfaces were parallel, the discs were then hot pressed under vacuum between tungsten carbide plates at a temperature ~40 °C above T_g. For the measurement, the samples were mounted on a motorised translation stage and the movement and data collection were controlled by computer. Measurements were made at 2 energies (between 50 and 200 nJ, chosen as appropriate for each glass composition) to confirm the reliability of n_2 calculated. Further details on the analysis of these samples are given by McCarthy.[22]

3.3. Raman scattering

A Horiba LabRAM HR Raman system with a 660 nm Laser-Quantum Ignis laser (187 mW set to 25% power) was used to collect Raman scattering data from the sample material. The samples were prepared by cutting a disc from the as-annealed glass rod and polished to a 1 μm finish. The data were collected using a 4 second exposure and accumulated over 10 scans. Repeat measurements at different points on each glass disc were made to ensure that the Raman spectra measured were representative of the whole glass. A background subtraction was performed on each spectrum before fitting was carried out.

3.4. ^{77}Se NMR

^{77}Se NMR spectra were recorded at room temperature on an Avance III 600 Bruker spectrometer at a Larmor frequency of 114.497 MHz using a 2.5 mm magic angle spinning (MAS) probe, spinning at 15 kHz. A spin echo pulse sequence was used to acquire the broad line that results from the distribution of isotropic chemical shifts expected for the glassy state. The echo delay was synchronised with the MAS period and set to 66.67 μs. The ^{77}Se π/2 pulse duration was 4 μs and the spectral width was 500 kHz. Acquisition commenced immediately after the π pulse in order to sample the whole echo to increase the signal-to-noise ratio. Given the low natural abundance of ^{77}Se (7.58%), up to 24 000 scans were required per spectrum, with a relaxation delay of 10 s. Chemical shifts are quoted relative to neat $(CH_3)_2Se$.

3.5. Neutron and X-ray total scattering

For total scattering using neutrons, the as-annealed glass rods were placed inside cylindrical vanadium containers, of inner diameter 10 mm, for the neutron scattering measurements. These vanadium containers were thin-walled, with a thickness of 25 μm, in order to reduce the magnitude of the experimental corrections required. The neutron diffraction patterns were measured using the GeM diffractometer[23] at the ISIS pulsed neutron and muon source (Rutherford Appleton Laboratory, Oxfordshire, UK). The data were normalised using a calibration measurement of an 8 mm vanadium rod and were reduced and corrected for attenuation and multiple scattering using standard Gudrun[24] and ATLAS[25] software to give the distinct scattering spectra, $i^N(Q)$. $i^N(Q)$ was fitted with a quadratic, of the form $A + BQ^2$, at low Q to extrapolate the data to $Q = 0$.

The X-ray data were collected at the Diamond Light Source (Rutherford Appleton Laboratory, Oxfordshire, UK) using the I15 beamline optimised for the collection of PDF data. The photon energy used for the experiment was 73 keV. The samples were powdered and placed in 1 mm diameter silica capillaries, and the scattering was detected using a Perkin Elmer 2D flat panel 1621 detector. The 2D data were reduced to 1D using Fit2D[26,27] and were corrected for detector attenuation as detailed by Skinner *et al.*[28] The 1D data were normalised using the Krogh-Moe and Norman method[17,18] and corrected for attenuation and multiple scattering using GudrunX[29] to produce the sharpened distinct scattering spectrum, $i^X(Q)$.

In both experiments, measurements of the empty instrument and empty container were made for data corrections. Once fully corrected $i^N(Q)$ and $i^X(Q)$ were Fourier transformed, using the Lorch modification function and a maximum momentum transfer, Q_{max}, of 35 Å^{-1} for neutron and 25 Å^{-1} for X-ray data, to give the total correlation functions, $T(r)$.

Predictions of the interatomic distances between nearest neighbour atoms were made using standard bond valence parameters.[30] The calculated bond lengths (presented in Table 2) were used as starting parameters when fitting $T(r)$. Simultaneous fitting to $T^N(r)$ and $T^X(r)$ was carried out using NXFit.[31]

The neutron diffraction data, in both reciprocal- and real-space, are available from the ISIS Disordered Materials Database.[55]

Table 2 Calculated interatomic bond lengths for all potential bonds in As–S–Se glasses. Distances are calculated using bond valence.[30] Bond lengths in bold are those that might be expected to be present in the glass (Se is two-coordinated and As is three-coordinated)

Coordination number	2.00	3.00	4.00
Bond type	Bond lengths		
As–S	2.11	**2.26**	2.37
As–Se	2.24	**2.39**	2.50
As–As	2.26	**2.41**	2.52
S–S	**2.07**	2.22	2.33
Se–S	**2.25**	2.40	2.51
Se–Se	**2.36**	2.51	2.62

4. Results

4.1. Sample characterisation

Densities ranged from 3.19 ± 0.04 g cm^{-3} for $As_{40}S_{60}$ to 4.55 ± 0.04 g cm^{-3} for $As_{40}Se_{60}$ (Table 3). The linear variation in density

Table 3 Compositional data for the seven As–S–Se glasses, as determined by XRF and EDX analysis, with density, non-linear refractive index, n_2, non-linear absorption coefficients, β, and Se–S coordination number measurements, n_{SeS}

Nominal composition at%	XRF composition at% (±3)	EDX composition at% (±1)	Density g cm^{-3} (±0.04)	T_g Onset (±2)	T_g Maximum gradient (±2)	n_2 ($\times10^{-18}$ m^2 W^{-1}) (±0.5)	β ($\times10^{-12}$ mW^{-1}) (±0.2)	n_{SeS} (±0.4)
$As_{40}S_{60}$	$As_{43}S_{57}$	$As_{40}S_{60}$	3.19	198	209	2.3	0.53	
$As_{40}S_{45}Se_{15}$		$As_{40}S_{45}Se_{15}$	3.59	190	200	2.3	1.0	4.4
$As_{40}S_{40}Se_{20}$	$As_{42}S_{39}Se_{19}$	$As_{38}S_{40}Se_{22}$	3.69	192	204	3.4	2.7	4.1
$As_{40}S_{30}Se_{30}$	$As_{39}S_{32}Se_{29}$	$As_{39}S_{30}Se_{31}$	3.91	189	199	4.5	2.0	3.6
$As_{40}S_{20}Se_{40}$	$As_{41}S_{20}Se_{39}$	$As_{38}S_{21}Se_{41}$	4.10	188	199	6.0	3.7	2.6
$As_{40}S_{15}Se_{45}$		$As_{40}S_{14}Se_{46}$		188	199	6.1	2.8	
$As_{40}Se_{60}$	$As_{39}Se_{61}$	$As_{39}Se_{61}$	4.55	170	176	10.5	2.8	0

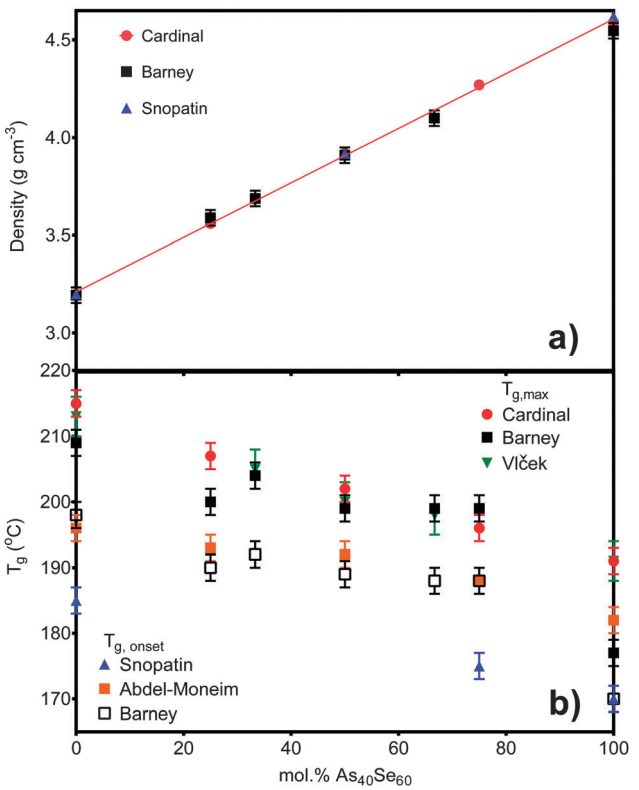

Fig. 1 (a) The density measurements for six of the samples in this study compared to literature values published by Cardinal *et al.*[3] and Snopatin *et al.*[5] The density for $As_{40}S_{15}Se_{45}$ is not shown as the sample size was too small to allow an accurate measurement. (b) The glass transition temperatures for all seven glasses are compared to the literature values published by Cardinal *et al.*[3] and Snopatin *et al.*[5] in addition to those published by Vlček *et al.*[6] and Wang *et al.*[32] The different results are grouped depending on the definition of T_g used.

with x, shown in Fig. 1a, suggests that there are no non-linear long range changes in the arrangement of the basic structural [$AsCh_3$] units as Se is substituted for S. T_g measurements are shown in Fig. 1b, calculated by two methods. The values of $T_{g,max}$ and $T_{g,onset}$, were found to vary non-linearly with the addition of $As_{40}Se_{60}$. There was a decrease in $T_{g,onset}$ of 8 °C on changing the glass composition from $As_{40}S_{60}$ to $As_{40}S_{45}Se_{15}$. However, as further selenium is added to the glass network, it was observed that $T_{g,onset}$ value remain constant, within error, until a composition of $As_{40}S_{15}Se_{45}$ is reached. On changing the composition of the glass from $As_{40}S_{15}Se_{45}$ to one with no sulfur at all, $As_{40}Se_{60}$, a further drop in $T_{g,onset}$ of 18 °C was observed.

The XRF and EDX results for glass composition were calculated using standardless calibration programs and are also given in Table 3. EDX measurements for each element were correct, to within 2 at%, at all times. This indicated that, within error, all the glasses had a stoichiometric composition $As_{40}Ch_{60}$. However, it should be noted that although the compositional analysis carried out by XRF is also consistent with the batched compositions, within error, the binary glass, $As_{40}S_{60}$, deviated most from the nominal compositions (3 at% excess As). It was expected that XRF would determine the composition of this glass with reasonable accuracy as it is comprise only two components. Therefore, while the batch compositions are assumed to be correct for subsequent analysis, the possibility that $As_{40}S_{60}$ was arsenic rich is considered in the discussion.

4.2. Raman

The Raman spectral bands, shown in Fig. 2a, are centred at 345 cm^{-1} for $As_{40}S_{60}$, characteristic of the vibration of As–S bonds, and 230 cm^{-1} for $As_{40}Se_{60}$, characteristic of As–Se bond vibrations.[2,3,9–11] The mixed chalcogen samples were composed of As–S and As–Se bonds and so exhibit both peaks. The effect of oscillator strength is shown in Table 4. The area of the As–S peak measured for $As_{40}S_{60}$ is ~50% of that measured for the As–Se peak in $As_{40}Se_{60}$. As a result, the relative intensities of the two peaks cannot be used directly to determine the relative amounts of As–S and As–Se bonds in the mixed chalcogen glasses. Fig. 2b shows the percentage variation in intensity of the As–Se and As–S peaks with x. The intensity of the As–Se peak, as Se was replaced by S, varied linearly, but the As–S peak intensity did not. A linear trend line fitted to the As–S peak intensities measured for x = 0–67 predicted that a Raman spectrum for a glass consisting of 85 mol% $As_{40}Se_{60}$ would exhibit no As–S peak.

4.3. ^{77}Se NMR

To check the consistency of the selenium environment with composition, ^{77}Se NMR spectra were collected for $As_{40}Se_{60}$ and $As_{40}S_{40}Se_{20}$ (x = 100 and 33) glasses. Gaussian peak fits to the spectra, shown in Fig. 3, were fixed at 380 ppm and the NMR spectra for both glasses could be simulated well with a single peak. A peak with a chemical shift of 380 ppm arises from Se atoms bonded to two arsenic atoms.[8]

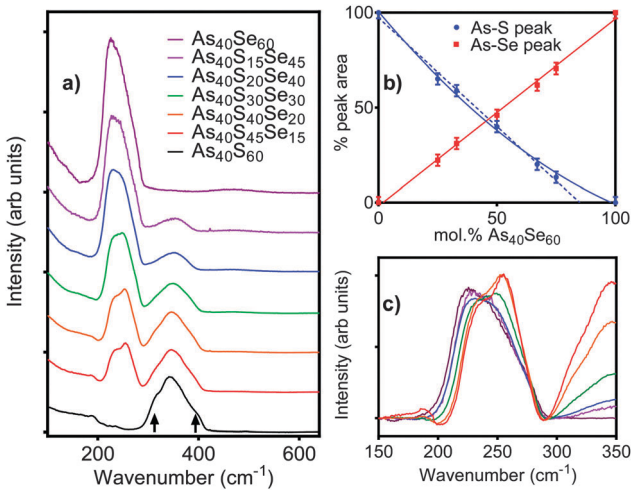

Fig. 2 (a) The Raman spectra for seven bulk chalcogenide glasses, collected at 660 nm. Arrows indicate the position of the shoulders on the As–S peak. (b) The relative areas of the As–S (blue) and As–Se (red) peaks with composition. The solid lines show the best fit through all the data points and the blue dashed line is a linear fit to the As–S peak intensities for $x < 67$. (c) A more detailed comparison of the changes in the As–Se peak shape with composition (key matches that in a). Each spectrum is scaled by the amount of $As_{40}Se_{60}$ present in the sample, x.

Table 4 The areas of As–Se and As–S bands in the Raman spectra obtained for each composition using a multi-peak fit to the peak manifold. Results are given as a % of the peaks observed in the end member glasses

Nominal composition at%	As–Se peak area as % of $As_{40}Se_{60}$ spectrum	As–S peak area as % of $As_{40}S_{60}$ spectrum
$As_{40}S_{60}$	0.0	100.0
$As_{40}S_{45}Se_{15}$	22.3	65.2
$As_{40}S_{40}Se_{20}$	31.1	59.0
$As_{40}S_{30}Se_{30}$	46.0	40.0
$As_{40}S_{20}Se_{40}$	61.9	20.1
$As_{40}S_{15}Se_{45}$	70.8	13.3
$As_{40}Se_{60}$	100.0	0.0

4.4. *Z*-scan measurements of n_2

Z-scan measurements of the non-linear refractive index, n_2, and non-linear absorption, β, are given in Table 3. There is a slow change in n_2 in sulfur rich glasses, varying from 2.3 ($\pm$0.5) $\times$ 10^{18} m^2 W^{-1} to 4.5 ($\pm$0.5) $\times$ 10^{18} m^2 W^{-1} as the composition is changed from $As_{40}S_{60}$ to $As_{40}Se_{30}S_{30}$ (x = 0–50). However, as the selenium content was increased, the rate of change accelerated, reaching a value of 10.5 ($\pm$0.5) $\times$ 10^{18} m^2 W^{-1} for $As_{40}Se_{60}$ (x = 100). Literature measurements for n_2 (ref. 3 and 4) are quoted relative to silica making direct comparison of values of n_2 difficult. To facilitate a comparison, Fig. 4a shows the values for n_2 measured by this study, along with those measured by Cardinal *et al.*,[3] Harbold *et al.*[4] and Wang *et al.*,[32] relative to the values of n_2 measured for $As_{40}S_{60}$. The relative change with x observed by all three studies is similar, with n_2 for $As_{40}Se_{60}$ being 4.0–4.5 times larger than $As_{40}S_{60}$. Fig. 4b shows that the variation in n_2 with x is not linear, but can be fitted with a second order polynomial equation.

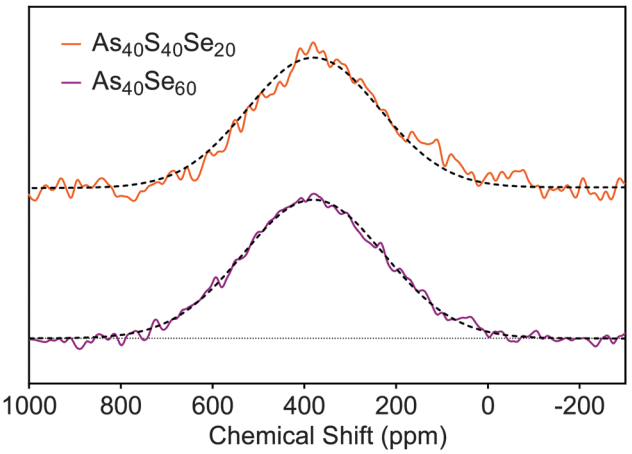

Fig. 3 ^{77}Se NMR spectra acquired for the $As_{40}Se_{60}$ and $As_{40}S_{40}Se_{20}$ samples. The solid lines are the experimental data, and the dashed lines are the peak fits.

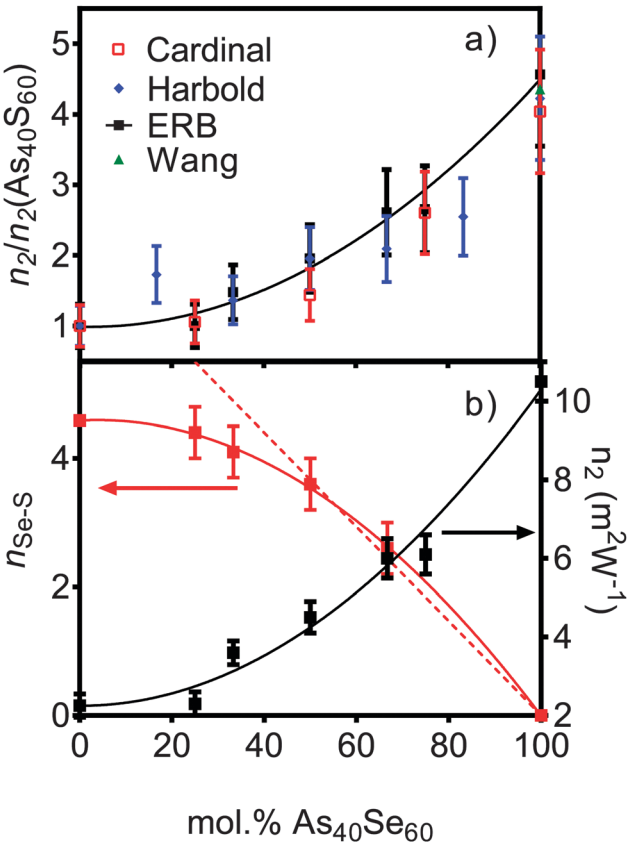

Fig. 4 (a) The variation in non-linear optical response of the series of $xAs_{40}Se_{60}\cdot(100 - x)As_{40}S_{60}$ glasses as measured in this study at 1.55 μm wavelength (black squares). The results are compared to literature results (right y axis) from Cardinal *et al.*[3] at 1.6 μm (red squares), Harbold *et al.*[4] at 1.55 μm and Wang *et al.*[32] at 1.55 μm. To allow direct comparison, the results are normalised to the n_2 value for $As_{40}S_{60}$. (b) The experimental values for n_2 (this study – black squares), with n_{SeS} values derived from $T^N(r)$ (red squares, x = 0 value is derived from the fit to experimental data) as a function of composition. The solid lines are the polynomial fits to the data. The dashed red line is the line of best fit to n_{SeS} for the x = 50, 67 and 100 mol% $As_{40}Se_{60}$ samples (when x = 0, y = 7.33).

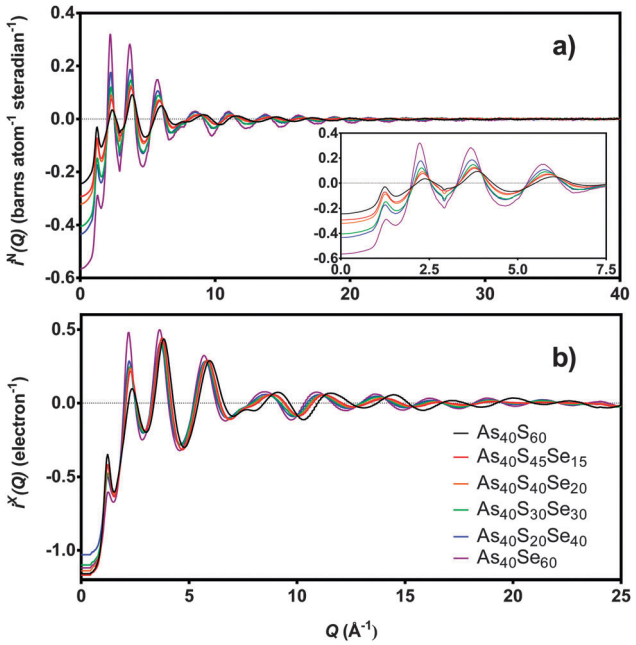

Fig. 5 (a) $i^N(Q)$ and (b) $i^X(Q)$ for six $x As_{40}Se_{60}\cdot(100 - x)As_{40}S_{60}$ samples. The insert shows the low Q region in more detail. $As_{40}S_{15}Se_{45}$ is not shown as sample was too small for scattering measurements.

4.5. Neutron and X-ray scattering

The distinct scattering patterns, measured using neutrons, $i^N(Q)$, and X-rays, $i^X(Q)$, are shown in Fig. 5 (except $As_{40}S_{15}Se_{45}$, which was not measured). All diffraction data exhibited a shift in the position of peaks to shorter Q with increasing selenium content. The exception was the position of the pre-peak at 1.26 Å^{-1}, which was unchanged (±0.3 Å^{-1}). The shift in peak position to shorter Q indicated an expansion of the glass network to accommodate the increase in average chalcogen size. The corresponding correlation functions, $T^N(r)$ and $T^X(r)$, are shown in Fig. 6. There were two well defined peaks at ~2.35 Å and 3.55 Å in the correlation functions; the former arose from As–Ch bonds and the latter from the shortest, non-bonded, distances for As···As/Ch···Ch. Some of these short As···As and Ch···Ch distances arose from the next nearest neighbours within an [$AsCh_3$] unit (Ch–As–Ch) or between two units (As–Ch–As), but an examination of the structure of crystalline $As_{40}Se_{60}$ (ref. 33) indicated that up to 50% of the contribution to n_{AsAs} may not be caused by As–Ch–As through-bonding, but rather from the close packing of structural units that are not directly connected.

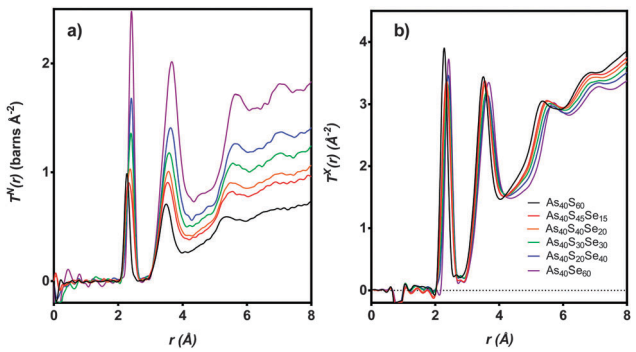

Fig. 6 $T(r)$ for six $x As_{40}Se_{60}\cdot(100 - x)As_{40}S_{60}$ samples as measured using (a) neutrons and (b) X-rays. $As_{40}S_{15}Se_{45}$ is not shown as sample was too small for scattering measurements.

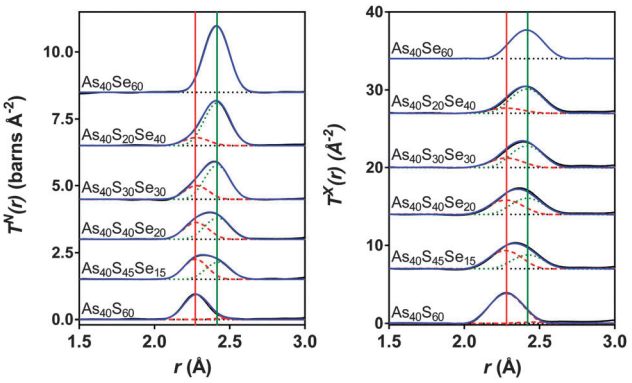

Fig. 7 Simultaneous fits to the neutron and X-ray diffraction data. The red dashed lines are the As–S peaks and the green dotted lines are the As–Se peaks. The solid red and green lines show the expected As-S and As-Se bond lengths respectively (see Table 2). The blue line is the sum of the fit and the black line is the experimental data. The black dotted lines show the baseline for each $T(r)$.

Fig. 7 shows simultaneous fits to the first peak in $T^X(r)$ and $T^N(r)$ for the $x As_{40}Se_{60}\cdot(100 - x)As_{40}S_{60}$ glass system. The fits required two peaks in order to model the As–S and As–Se bonds. The positions, widths and areas of the peaks were allowed to vary freely and the fit parameters are given in Table 5. The As–Se and As–S peak positions were all within 0.01 Å of the bond lengths for As–S and As–Se (2.271 ± 0.001 Å and 2.412 ± 0.001 Å) found by fitting the end member glasses. Furthermore, the coordination numbers for the two bond types, n_{AsS} and n_{AsSe}, were within 0.05 of the predicted average coordination numbers calculated from the glass composition (Table 5), yielding a total coordination number for arsenic in all of the glasses within the range of 3.0 ± 0.1.

5. Discussion

5.1. Density, glass transition temperature and composition

The measured densities for glasses in the system $x As_{40}Se_{60}\cdot(100 - x)As_{40}S_{60}$ shown in Fig. 1a agreed, within error

Fig. 6 shows that the first peak in the correlation functions, $T^N(r)$ and $T^X(r)$, for $As_{40}S_{60}$ was centred at ~2.27 ± 0.01 Å, while the corresponding peak for $As_{40}Se_{60}$ was centred at ~2.41 ± 0.01 Å. The intermediate ternary glasses, which were composed of As–S and As–Se bonds, exhibited a broader first peak in $T(r)$. The average peak position shifts between the distances observed in $T(r)$s for $As_{40}S_{60}$ and $As_{40}Se_{60}$ as Se was substituted for S in the glass network. The positions of the As–Ch and Ch···Ch peaks in the correlation functions for $As_{40}S_{60}$ (2.27 and 3.42 Å) and $As_{40}Se_{60}$ (2.41 and 3.62 Å) were consistent with Ch–As–Ch bond angles of ~100°, which is in good agreement with that expected for the trigonal pyramid environment of a three-coordinated lone-pair ion.[34]

Table 5 The parameters obtained from simultaneous fits to the As–Ch peaks in X-ray and neutron $T(r)$s. The bond lengths, r, peak widths, σ, and coordination numbers, n_{AsCh}, are given, along with the expected coordination numbers, for each sample. The two peak fit for $As_{40}S_{60}$ is treated as both two As–S distances, and As–S and an As–As distance

Composition	Correlation	r (Å)	σ (Å)	n_{AsCh}	Calculated n_{AsCh}
$As_{40}S_{60}$	As–S_1	2.271(1)	0.0585(2)	2.86(3)	3
	As–S_2 (*As–As*)	2.467(3)	0.029(1)	0.11(3) (*0.09(3)*)	
	As–S (*As–X*) total	2.97(5) (*2.95(5)*)			
$As_{40}S_{45}Se_{15}$	As–S	2.273(2)	0.061(1)	2.24(3)	2.25
	As–Se	2.424(2)	0.074(1)	0.74(3)	0.75
	As–Ch total	2.98(5)			
$As_{40}S_{40}Se_{20}$	As–S	2.277(2)	0.066(1)	1.97(3)	2
	As–Se	2.419(2)	0.069(1)	0.97(3)	1
	As–Ch total	2.94(5)			
$As_{40}S_{30}Se_{30}$	As–S	2.279(2)	0.061(1)	1.49(3)	1.5
	As–Se	2.416(2)	0.065(1)	1.48(3)	1.5
	As–Ch total	2.97(5)			
$As_{40}S_{20}Se_{40}$	As–S	2.277(2)	0.068(1)	0.95(3)	1
	As–Se	2.417(2)	0.069(1)	1.95(3)	2
	As–Ch total	2.90(5)			
$As_{40}Se_{60}$	As–Se	2.412(1)	0.0659(2)	2.93(3)	

($\pm$0.04 g cm^{-3}), with previously work by Cardinal *et al.*[3] and Snopatin *et al.*[5] and are a first indication that the glass compositions did not deviate from those batched. In contrast, the measurements for the glass transition temperature do not agree with those reported by Cardinal *et al.* and Snopatin *et al.* for the same samples.

When comparing the glass transition temperatures, T_g, measured in this study with those in the literature (Fig. 1b), it is important to consider how T_g is defined by different researchers. Cardinal *et al.* clearly state that they define T_g as the point in the region of glass transition with the maximum gradient.[3] Data published by Vlček *et al.*[6] yield very similar results to Cardinal *et al.* and, though it is not explicitly stated, we have assumed that they used a similar definition of T_g. In contrast, T_g values measured by Abdel-Moneim were reported to be calculated using the onset T_g definition.[35] The results published by Snopatin *et al.* for comparable compositions are consistently lower in temperature than all other data sets,[5] but the equivalence between the density values given by Cardinal *et al.* and Snopatin *et al.* suggests that this difference in reported glass temperatures may arise from a change in definition of T_g rather than because of any major differences in sample composition. The above consideration of results from three different published studies highlights that the definition of T_g used has a significant impact on the values reported, with a difference of $\sim$10 °C between the $T_{g,onset}$ and $T_{g,max}$ for the results in Table 3. Therefore the definition must be clearly stated along with measurements if the results published are to be useful for future researchers. Fig. 1b shows a comparison of $T_{g,onset}$ and $T_{g,max}$ measured in this study with the literature. $T_{g,max}$ values gave generally good agreement with Cardinal *et al.* and Vlček *et al.*, while the $T_{g,onset}$ values were closer to those of Abdel-Moneim.[35]

The glass transition temperatures published by Cardinal *et al.*,[3] Vlček *et al.*[6] and Snopatin *et al.*[5] all decrease linearly as $As_{40}Se_{60}$ is added to $As_{40}S_{60}$. Five of the seven $T_{g,max}$ results agreed, within error, with those of Cardinal *et al.* and Vlček *et al.*, who observe only a $\sim$23 °C change in $T_{g,max}$ across the compositional range. However, the two exceptions, the transition temperatures for $As_{40}S_{45}Se_{15}$ and $As_{40}Se_{60}$, have a considerable impact on the interpretation of the data. An analysis of the glass transition temperatures obtained in this study suggest that T_g does not vary linearly in mixed anion glasses, but is instead relatively constant across a wide compositional range. The invariance in the glass transition temperature for glasses in a compositional range from $As_{40}S_{45}Se_{15}$ to $As_{40}S_{15}Se_{45}$ suggests that the mixed phase glasses maintain a similar structural motif. Furthermore, the $T_{g,max}$ values for these glasses were closer to that of $As_{40}S_{60}$ than $As_{40}Se_{60}$ indicating that the glass relaxation behaviour is more similar to the sulfide glass than the selenide. Careful analysis of the composition and homogeneity of the glasses is vital to ensure that this interpretation is accurate. The presence of phase separation in the $As_{40}Se_{60}$ glass, for example, would result in a mix of As–As and Se–Se bonds that could affect T_g. Literature indicates that moving away from the stoichiometric composition, and therefore increasing the number of homopolar bonds, lowers T_g.[36,37] However, it should be noted that a review of T_g temperatures for $As_{40}Se_{60}$, reported in the Sciglass software,[38] gave a wide variation in results, ranging from 150 °C to 200 °C, and yielded a mean T_g of 181 °C with a standard deviation of 11 °C. The "anomalous" T_g values reported for $As_{40}Se_{60}$ in this study were both within this error range.

Compositional analyses of all of the glasses agreed with the batched compositions, within the error of the techniques used (Table 3). The composition for $As_{40}S_{60}$ determined using XRF (Table 3) was most disparate from the batched composition, suggesting that there may have been a small excess of arsenic in the glass. If this were true, the glass would no longer be

comprised of only [AsS_3] units, but must have included a number of As–As bonds. The $As_{40}Se_{60}$ glass, which has an anomalous glass transition temperature, is reported to have a composition of $As_{39}Se_{61}$ and so is considered to be stoichiometric in all analysis.

5.2. Short range order and homopolar bonds

The glass compositions used in this study have been designed so that, in an ideal glass, each As atom was bonded to three Ch atoms, and each Ch is bonded to two As atoms. Therefore, if homopolar bonds were present, they would have arisen from either an excess of As (as suggested by XRF compositional analysis for $As_{40}S_{60}$), or from phase separation resulting in As rich and Ch rich regions (see, for example, work by Petri *et al.*[39] and Georgiev *et al.*[40]). Phase separation can be intrinsic to the glass, or arise from a lack of inhomogeneity in the glass melt. The structural information gained from Raman spectroscopy, ^{77}Se NMR and neutron and X-ray total scattering were therefore interrogated for evidence of homopolar bonds before stoichiometry ($As_{40}Ch_{60}$) was accepted.

5.2.1. Evidence for homopolar bonds in $As_{40}S_{60}$. XRF analysis of the $As_{40}S_{60}$ glass indicated that the true composition of the glass was $As_{43}S_{57}$. However, this result was not considered reliable because the Raman spectrum in Fig. 2a and $T^N(r)$ in Fig. 6a did not match the published results for glasses with compositions of $\sim As_{42}S_{58}$.[9,13,41] Fig. 2a shows that a peak manifold, centred at $\sim$350 cm^{-1}, was the dominant contribution to the Raman spectrum of $As_{40}S_{60}$, as expected for As–S bonds. However, there were also weak bands observable at 188, 233 and 498 cm^{-1} that may indicate the presence of a very small number of As–As and S–S bonds in the glass.[2,3,9–11] For example, peaks at $\sim$500 cm^{-1} in the Raman spectra have been assigned by Golovchak *et al.* to sulfur dimers of the form As–S–S–As.[9] There was no evidence in the neutron or X-ray correlation functions (Fig. 6a) of S–S bonds, which would have contributed a peak in $T(r)$ at 2.04 Å (see Table 2 and ref. 13), but it should be noted that sulfur scatters both X-ray and neutrons very weakly in contrast to arsenic.

Georgiev *et al.*[40] attributed the weak features, observed in the Raman spectrum of $As_{40}S_{60}$, at 188 and 233 cm^{-1} to the vibrations of [As_4S_4] molecules, which are comprised of As–S and As–As bonds. Using this assignment, and the intensity of the two bands, they estimated that 7% of the As bonds in bulk $As_{40}S_{60}$ glass were homopolar.[40] The correlation functions obtained using neutrons and X-rays, $T^N(r)$ and $T^X(r)$, were carefully analysed to determine where this concentration of As–As bonding is reasonable.

The simultaneous fits to the correlation functions, $T^N(r)$ and $T^X(r)$, for $As_{40}S_{60}$ (Fig. 7) required two peaks to model the distribution of bond lengths fully. The parameters for the fit are given in Table 5. The peak positions, 2.271 ± 0.001 Å and 2.467 ± 0.001 Å, could be interpreted as arising from a distribution of As–S bond lengths, or from As–S and As–As bonds, respectively (see Table 2 and ref. 13). A consideration of the total arsenic coordination number does not aid in determining which interpretation is correct because both yield a total coordination number of 3, within the error of the experiment. The width of the peak fitted at 2.467 Å was 0.029 ± 0.001 Å. This is significantly narrower than the widths of the As–S or As–Se peaks given in Table 5 ($\sim$0.06 Å) and indicates that the peak is not a real measure of a correlation. Furthermore, the second peak is also at a distance that is more than 0.06 Å shorter than the As–As bond length measured using neutrons[13] and K edge As EXAFS[42] in As rich glasses. Based upon this interpretation, it can be proposed that the slight asymmetry of the As–S peak shape in the neutron correlation function (Fig. 6) arises from a distribution of As–S bond lengths in the glass. Similar asymmetric bond distributions have been observed in correlation functions for oxide glasses containing lone pair cations, such as As, when a $Q_{max} \geq 30$ Å^{-1} is used for the Fourier transform (*i.e.* [PbO_3][43] and [SbO_3][44]). For example, a similar two peak fit to the Pb–O distribution in PbO–Al_2O_3 glasses yielded Pb–O peak positions of $\sim$2.25 and 2.47 Å.[43] In contrast, the presence of small peaks in the Raman spectra at $\sim$200 cm^{-1} supports the interpretation that the shoulder arises from a small number of As–As distances in the glass. An As–As coordination number of 0.09 ± 0.03 indicates that between 2 and 4% of arsenic bonds are homopolar, slightly less than the number predicted by Georgiev *et al.*[40] In summary, the measured coordination number of arsenic is close to the expected value of three, and there is some evidence for a small number of As–As bonds. However, the presence of homopolar bonds at these concentrations would have a negligible effect on further analysis and the glass shall be considered as stoichiometric and comprised solely of [AsS_3] in the remainder of the discussion. For a more detailed study of As–As bonds in $As_{40}S_{60}$ careful fitting of $T^N(r)$ for a series of As_xS_{100-x} glasses is required to establish robust parameters for S–S, As–S and As–As peaks.

5.2.2. Evidence for homopolar bonds in Se containing glasses. The close similarity of atomic mass and radius for As and Se makes the determination of homopolar Se–Se bonds in the presence of As–Se bonds more difficult than identifying S–S bonds in the presence of As–S. Bond valence parameters[30] were used to calculate the expected bond lengths for an arsenic atom bonded to three Se or As atoms, and a selenium atom bonded to two Se atoms. The results are given in Table 2 and the three distances, differing by less that 0.05 Å, would not resolvable in a neutron or X-ray correlation function. Furthermore, the vibrational frequencies of As–Se, Se–Se and As–As bonds are also unresolvable by Raman spectroscopy. Therefore, an alternative determination of the local environment of Se in the arsenic selenide glasses was used. ^{77}Se NMR studies of arsenic selenide based glasses carried out by Bureau *et al.*[7,8] and Delaizir *et al.*[45] have identified three chemical shifts, 380, 560 and 820 ppm, in ^{77}Se NMR spectra. These shifts have been assigned to As–**Se**–As, As–**Se**–Se and Se–**Se**–Se environments, respectively. The ^{77}Se NMR spectra for $As_{40}Se_{60}$ and $As_{40}S_{40}Se_{20}$, shown in Fig. 3, have been fitted with a single peak centred at 380 ppm, indicating that both glasses are primarily comprised of As–**Se**–As environments. The glasses in this study are therefore concluded to have a high degree of chemical order; Se is predominantly found in [$AsCh_3$] units, with few or no Se–Se bonds in the amorphous $As_{40}Se_{60}$ and $As_{40}S_{40}Se_{20}$. This conclusion is

supported by Bureau and colleagues who used a ^{77}Se NMR 2D Carr–Purcel–Meiboom–Gill (CPMG) pulse program to measure Se environments in As–S–Se glasses.[46]

5.2.3. Local structure of xAs$_{40}$Se$_{60}$·(1 − x)As$_{40}$S$_{60}$ glasses determined by neutron and X-ray $T(r)$s. The results outline in Sections 5.2.1 and 5.2.2 indicate that the glasses are predominantly composed of As–Se and As–S bonds, and these assignments were used to interpret the fits to the neutron and X-ray correlation functions, show in Fig. 7. Table 5 gives the calculated arsenic coordination numbers, n_{AsCh}, obtained from these fits, along with the predicted values calculated from the composition of each glass. Prediction and experiment agreed, within error. The different scattering lengths of As, S and Se, given in Table 1, indicate that the presence of a significant number of As–As or Se–Se bonds in the glass would change the area of the first peak in the correlation functions, leading to a poorer agreement between the predicted and measured coordination numbers. Therefore, the achieved agreement between expected and measured coordination numbers gave a further indication that As–Ch linkages were the dominant bonding mechanism in these glasses. In conclusion, combining the compositional analysis, carried out using XRF and EDX, with the analysis of the Raman spectra, ^{77}Se NMR spectra and neutron and X-ray correlation functions, indicated that the glasses in this study were stoichiometric. The first peak in the neutron and X-ray correlation functions was considered to be comprised of As–S and As–Se bonds, only.

5.3. Changes in network connectivity with composition

5.3.1. Raman. The intensities of the As–S band (270–420 cm^{-1}) in the Raman spectra (Fig. 2a) for the seven glass compositions are given in Table 4. The fractional change in intensity of the As–S band with x is shown in Fig. 2b with a linear fit to the results. The fit indicated that there should be no contribution to the Raman spectra from an As–S peak when $x \geq 85$ in xAs$_{40}$Se$_{60}$·(100 − x)As$_{40}$S$_{60}$ glasses. However the intensity of the As–S band at ∼350 cm^{-1} was distorted by the presence of shoulders to either side of the main peak. These are labelled with black arrows in Fig. 2a. Wagner *et al.*[41] attributed these shoulders to vibrations between [AsS$_3$] units (*i.e.* [S$_2$As]–S–[AsS$_2$]). The As–S band in the experimental Raman spectra, shown in Fig. 2a, narrowed as S was replaced with Se until a composition of As$_{40}$S$_{20}$Se$_{40}$ was reached, indicating a decrease in intensity of the shoulder bands; the widths of the As–S peaks in Raman spectra for As$_{40}$S$_{20}$Se$_{40}$ and As$_{40}$S$_{15}$Se$_{45}$ (x = 67 and 75 respectively) showed no change (Fig. 2a). By using two lines to fit the As–S peak intensities in Fig. 2b, one to the x = 0–50 peak intensities and one to the x = 67–100 values (where x = 100 is an As$_{40}$Se$_{60}$ glass with no As–S peak), a more accurate measure of the sulfur concentration at which [AsS$_3$] units are no longer directly connected could be obtained from the intersection of the two lines. This occurred at x = 70 (As$_{40}$S$_{18}$Se$_{42}$). If the interpretation that the shoulders in the spectral band arise from bonded [AsS$_3$] units is correct, they would not be expected for compositions beyond ∼33% As$_{40}$Se$_{60}$. At this composition, the average arsenic unit would be [AsS$_2$Se]. The persistence of intensity in the shoulders to ∼70 mol% As$_{40}$Se$_{60}$ suggests that either the interpretation is incorrect, or that [AsS$_3$] units are present in the glass in much higher concentrations than would be expected by random chalcogen mixing.

Fig. 2c shows the As–Se peak manifold in detail. The Raman spectra have been scaled by the atomic fraction of Se present in the glass to allow a direct comparison the peak intensities and shape. If all Se atoms are bonded to As, the area of the bands in Fig. 2c should be invariant with composition. The linear relationship between x and peak area in Fig. 2b shows this to be true. The average [AsCh$_3$] structural unit in an As$_{40}$S$_{60}$ glass changes with the addition of As$_{40}$Se$_{60}$ from [AsS$_3$], *via* the formation of [AsSeS$_2$] and [AsSe$_2$S] units as Se replaces S in the glass network, until all As atoms are in [AsSe$_3$] units. A clear shift in the position of the maximum intensity of the As–Se band to lower wave numbers was observed as Se was added to the glass. Freitas *et al.*[11] and Li *et al.*[10] have previously attributed this red shift to a change in the next nearest neighbours for the selenium atoms. It should be noted that the peak manifolds at ∼250 cm^{-1} for As$_{40}$S$_{45}$Se$_{15}$ and As$_{40}$S$_{40}$Se$_{20}$ (x = 25 and 33) were similar, indicating that there was little change in the local Se environment at these two compositions.

5.3.2. Ch···Ch coordination numbers determined from correlation functions. It is possible to estimate the correlation function for a ternary As–S–Se glass using a weighted sum of the correlation functions for the binary glasses. A weighted function can be calculated by summing $T^{\mathrm{N}}(r)$ for the two binary glasses, As$_{40}$S$_{60}$ and As$_{40}$Se$_{60}$, in proportions to match the composition of each ternary glass, xAs$_{40}$Se$_{60}$·(100 − x)As$_{40}$S$_{60}$. However, this sum is only an approximation for $T^{\mathrm{N}}(r)$ for a ternary glass because As$_{40}$S$_{60}$, and As$_{40}$Se$_{60}$, are solely composed of [AsS$_3$], and [AsSe$_3$], units. Therefore, even if a weighted sum of the As···As and As···Ch correlations in As$_{40}$S$_{60}$ and As$_{40}$Se$_{60}$ glasses were a good approximation for the corresponding correlations in the mixed glasses, it cannot properly account for the Ch···Ch distances that arise from the presence of [AsS$_2$Se] and [AsSSe$_2$] units. Differences between the experimental correlation function and the weighted sum would become apparent in the region of the second peak in $T^{\mathrm{N}}(r)$, where the weighted Ch···Ch sum will over estimate the number of Se···Se and S···S correlations and neglect Se···S correlations. As the scattering length of S is significantly less than Se (Table 1), the weighted sum will have a more intense contribution from Ch···Ch correlations than is measured experimentally.

The experimental neutron correlation functions, $T^{\mathrm{N}}(r)$, for four ternary glasses are shown in Fig. 8 with the calculated weighted correlation functions. There was excellent agreement between the experimental data and weighted sum over the distance ranges 0–3.2 Å and 4.25–5.4 Å. For each glass sample, the difference between the experimental correlation function and the calculated weighted sum in the region of the first peak in $T^{\mathrm{N}}(r)$ was of the same order as the noise in the low r region. The first significant peak in the residual, attributed to Se···S distances, was observed at ∼3.75 Å and is narrow and well defined. The As$_{40}$S$_{30}$Se$_{30}$ glass exhibits the largest residual, because this is the composition where the potential for mixing

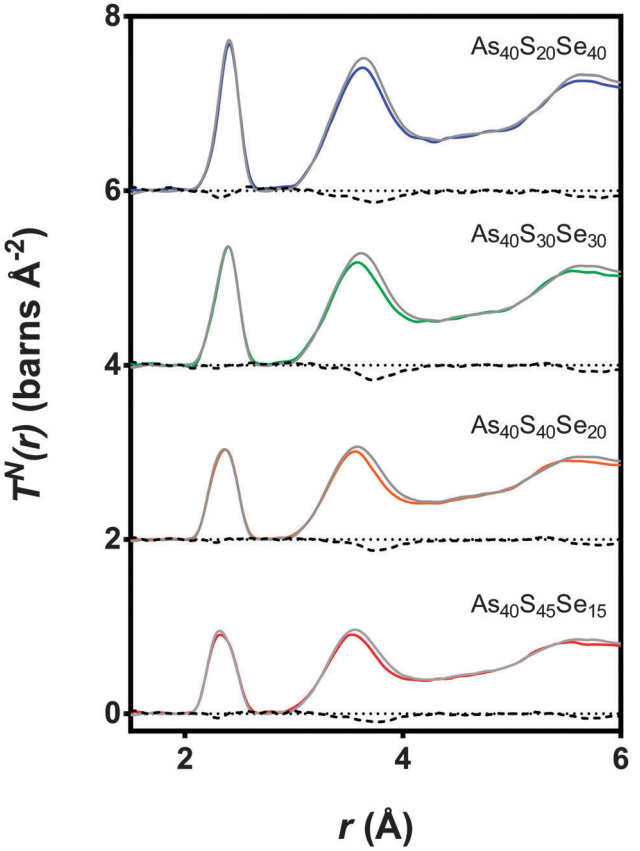

Fig. 8 The $T^N(r)$ data for four mixed As–S–Se samples (coloured lines) along with the expected spectra (grey line) calculated from a ratio of $T^N(r)$ for the two end member glasses ($As_{40}S_{60}$ and $As_{40}Se_{60}$). The differences between the measured and calculated spectra are shown using a black dashed line.

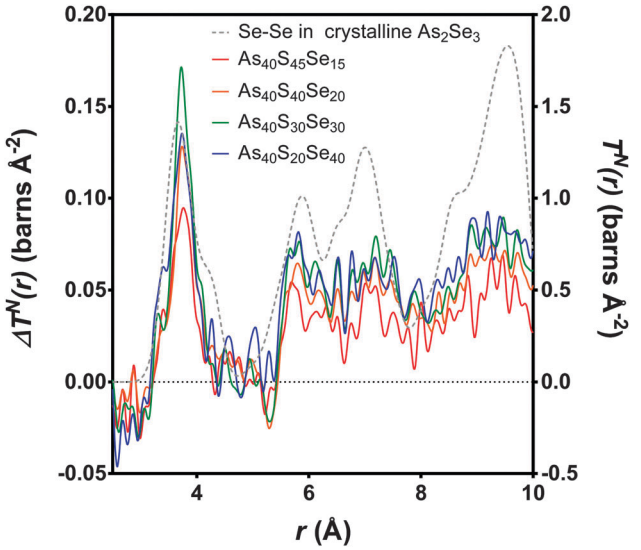

Fig. 9 The differences, ($\Delta T^N(r)$) as calculated in Fig. 8, between the experimental $T^N(r)$ and the weighted sum (coloured lines, left y-axis). The peak with the maximum intensity is the $As_{40}S_{30}Se_{30}$ glass, where the potential for mixing is at the maximum. The Se–Se partial correlation function is simulated for crystalline $As_{40}Se_{60}$ (ref. 33) (dashed grey line, right y-axis).

is maximised. Fig. 9 compares the differences between the experimental Se···S correlation and a calculated partial correlation for Se···Se distances (calculated from the reported crystal structures using the XTAL program[47]) in crystalline $As_{40}Se_{60}$.[33] There is close agreement between the first peak maximum for this simulation (3.71 Å) with the residuals (3.75 Å) and a general agreement in the shape of the residuals with the Se···Se partial correlation function over the range of 0–10 Å. This supports the hypothesis that the differences shown in Fig. 9 arose from a Ch···Ch correlation.

n_{SeS} values for each glass containing selenium were calculated by integrating the area of the peaks at ~3.75 Å in Fig. 9 and using eqn (11). The results are given in Table 3 and shown in Fig. 4b. If the Se and S anions were evenly distributed throughout the glass, a linear variation would be expected. A linear fit was made to n_{SeS} for glasses containing ≥50 mol% $As_{40}Se_{60}$, and is shown as a red dashed line in Fig. 4b. An extrapolation of this linear fit to $x = 0$ indicated that a single Se atom in an arsenic sulphide glass would have 7.3 sulfur neighbours, n_{SeS} = 7.3. This is close to n_{SeSe} = 7.33, calculated from the crystal structure of crystalline $As_{40}Se_{60}$,[33] when using a maximum Se···Se distance of 4.0 Å. The good agreement between the extrapolated value for n_{SeS} in the $As_{40}S_{60}$ and n_{SeSe} in crystalline $As_{40}Se_{60}$ indicated that the change in n_{SeS} was directly dependent on the total number of sulfur atoms in the glass. Therefore, selenium and sulfur atoms were randomly mixed when >50% of Ch atoms are selenium. However, Fig. 4b shows that values for n_{SeS} deviated from this linear correlation when <50% of the chalcogen atoms in the glass were selenium. To achieve a good fit to all values of n_{SeS} a second order polynomial was required. The intersection of this new fit with $x = 0$ occurred at 4.6. Such a markedly non-linear variation in n_{SeS} with composition suggested that either there was a preference for like atoms to cluster when there was a high concentration of sulfur in the glass, or that the average number of anions around the Se atom decreased from 7.3 to 4.6 as the amount of sulfur in the glass was increased from 0 to 60 at%. Conclusive evidence in favour of either suggestion is lacking. However, if the total number of Ch atoms around selenium decreased as sulfur was added to the glass, a corresponding expansion of the glass network would be expected. Instead, the shift in peak positions in $i^N(Q)$, shown in Fig. 5a, indicated that a *network contraction* occurs with increased sulfur content.

The interpretation of the Raman spectra in Section 4.3.1 supports the suggestion that n_{SeS} varies non-linearly with x. The shape of the As–Se band in the Raman spectra is strongly influenced by the surrounding environment. However, the shape of the As–Se peaks in Fig. 2c for $As_{40}S_{45}Se_{15}$ and $As_{40}S_{40}Se_{20}$ are very similar. This suggests that the local environment of the As–Se bonds was not changing as fast as would be expected if S and Se atoms were mixing randomly in the glass. Furthermore, the non-linear change in the intensity of the As–S peak in the Raman spectra suggested a preference for [AsS_3] units to persist in the glass to higher concentrations than random mixing would allow. In summary, the combination

of Raman and total scattering data indicates that there may be preferential clustering of selenium and sulfur in $x As_{40}Se_{60}\cdot(100-x)As_{40}S_{60}$ glasses, when there is a high concentration of the sulfur in the glass. As a selenium atom has a radius that is ~20% larger than sulfur,[48] this proposed clustering could be driven by an inability for a network of [AsS_3] units to accommodate easily the larger Se atoms.

5.4. A comparison of glass structure with physical properties

The results presented here, coupled with the literature, show that n_2 varies non-linearly with composition in this glass system.[3,4,49] Several theories have been put forward to explain the structural changes that underpin this non-linear response. Nasu *et al.*[50] related an increase in non-linear optical susceptibility, $\chi^{(3)}$ (related to n_2) to a denser glass network, highlighting that the low $\chi^{(3)}$ measured for $GeSe_4$ corresponds to a high molar volume. However, this is not consistent with the glass system studied here, where the molar volume and n_2 both increased as selenium atoms were doped into the network. More recent work by Harbold *et al.*[4] showed that there is a relationship between the band gap energy, E_g, and n_2. n_2 was shown to increase rapidly when the photon energy of the laser was $>0.5E_g$. Sanghera *et al.*[49] explicitly related n_2 with this normalised photon energy. However, it should be noted that the band gap energy and the onset of the absorption edge, λ_{gap}, also showed evidence of non-linear variation with composition.[3,49] Therefore, we suggest that the same changes in the glass structure affect both λ_{gap} and n_2. Petit *et al.*[51] showed an inverse relationship between the density of lone-pairs in the glass and n_2. However, this is in direct conflict with the accepted understanding that lone-pairs enhance n_2 in heavy metal oxide glasses (see ref. 52 for example). Harbold *et al.* highlighted this inconsistency and demonstrated that it is possible to maintain constant λ_{gap} and n_2 values for selected glasses in the Ge–As–Se system that exhibit different lone pair densities.[53]

From the brief discussion above, it is clear that the relationship between n_2, λ_{gap}, and glass structure is complicated and remains unresolved. The results of this study suggest an alternative structural origin for the non-linear variation in n_2 with x in the $x As_{40}Se_{60}\cdot(100-x)As_{40}S_{60}$ glass system. Fig. 10 shows a linear relationship between n_2 and n_{SeS}. We therefore propose that the variation in n_2 in this series of glasses is related to the arrangement of the chalcogen atoms in the glass. The variation in n_{SeS} only varied linearly, indicating a well-mixed glass, when $x > 0.5$. For glasses containing low concentrations of Se, there was evidence that the Se and S atoms preferentially cluster, which may result in a sublinear change in the non-linear refractive index of the glass. Work by Maklad *et al.* supports this interpretation,[54] as follows. Careful observation of i absorptions in the $x As_{40}Se_{60}\cdot(100-x)As_{40}S_{60}$ glass system indicated that the expected vibrations from [AsS_2Se] and [$AsSSe_2$] units are missing from an x = 40 mol% $As_{40}Se_{60}$ glass, and are only weakly present in an x = 93 mol% $As_{40}Se_{60}$ glass. The lack of vibrations from mixed units has been interpreted as a sign of non-random distribution of the chalcogens in these glasses and suggests that [AsS_3] and [$AsSe_3$] units form in preference to mixed units such as [AsS_2Se], when Se is present in low concentrations. This is in good agreement with the structural results presented here, which suggests that full mixing of the chalcogen atoms does not occur until ~50 mol% $As_{40}Se_{60}$ is present. Furthermore, the thermal analysis suggests that the mixed chalcogen glasses retain a more sulfide-like relaxation behaviour across the compositional range.

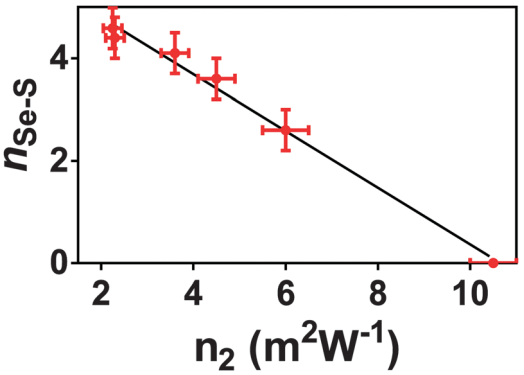

Fig. 10 n_{Se-S} plotted against n_2. The relationship between these two glass properties varies linearly. n_{Se-S} is, necessarily, zero for $As_{40}Se_{60}$, and the value for $As_{40}S_{60}$ is calculated from the second order polynomial fit in Fig. 4b.

6. Conclusions

A series of $x As_{40}Se_{60}\cdot(1-x)As_{40}S_{60}$ glasses, where x = 0, 25, 33.3, 50, 66.7, 75 and 100 mol% $As_{40}Se_{60}$, was investigated. Values of n_2, measured using Z-scan, were found to vary between $2.3(5)\times10^{18}$ m^2 W^{-1} for $As_{40}S_{60}$ to $10.5(5)\times10^{18}$ m^2 W^{-1} for $As_{40}Se_{60}$ and show a nonlinear variation with composition that was modelled using a second order polynomial equation. These results are in reasonable qualitative agreement with the trends in n_2 reported elsewhere. Through careful analysis of total correlation functions, obtained using neutrons and X-rays, it has been shown that there is a lower than expected number of sulfur atom nearest neighbours around a selenium atom in glasses containing ≤50 mol% $As_{40}Se_{60}$. The variation of n_{SeS} with x requires a second order polynomial fit to the data and this non-linear variation is attributed to the clustering of chalcogens in the glass. The observed variation in n_{SeS} was shown to have a linear relationship with n_2, and it is suggested that the spatial distribution of chalcogen atoms in the glass is a structural factor contributing to the non-linear changes in n_2 with composition. To be able to investigate the medium range structure of this As–S–Se glasses and determine the partial correlation functions for Ch···Ch correlations more fully structural modelling methods, such as Molecular Dynamics and Reverse Monte Carlo, will be used.

Acknowledgements

Experiments at the ISIS Pulsed Neutron and Muon Source were supported by a beamtime allocation (RB1120102) from

the Science and Technology Facilities Council. Special thanks is given to Professor Alex Hannon for support during the experiment. We also thank Diamond Light Source for access to Beamline I15.

References

1 A. Popescu, *Non-Crystalline Chalcogenicides*, Kluwer Academic Publishers, Dordrecht, The Netherlands, 2000.
2 F.-Y. Lin, O. Gulbiten, Z. Yang, L. Calvez and P. Lucas, *J. Phys. D: Appl. Phys.*, 2011, **44**, 045404.
3 T. Cardinal, K. A. Richardson, H. Shim, A. Schulte, R. Beatty, K. Le Foulgoc, C. Meneghini, J. F. Viens and A. Villeneuve, *J. Non-Cryst. Solids*, 1999, **256–257**, 353.
4 J. M. Harbold, F. Ö. Ilday, F. W. Wise, J. S. Sanghera, V. Q. Nguyen, L. B. Shaw and I. D. Aggarwal, *Opt. Lett.*, 2002, **27**, 119.
5 G. E. Snopatin, V. S. Shiryaev, V. G. Plotnichenko, E. M. Dianov and M. F. Churbanov, *Inorg. Mater.*, 2009, **45**, 1439.
6 M. Vlček, A. V. Stronski, A. Sklenař, T. Wagner and S. O. Kasap, *J. Non-Cryst. Solids*, 2000, **266–269**(Part 2), 964.
7 B. Bureau, J. Troles, M. Le Floch, F. Smektala and J. Lucas, *J. Non-Cryst. Solids*, 2003, **326**, 58.
8 B. Bureau, J. Troles, M. LeFloch, F. Smektala, G. Silly and J. Lucas, *Solid State Sci.*, 2003, **5**, 219.
9 R. Golovchak, O. Shpotyuk, J. S. McCloy, B. J. Riley, C. F. Windisch, S. K. Sundaram, A. Kovalskiy and H. Jain, *Philos. Mag.*, 2010, **90**, 4489.
10 W. Li, S. Seal, C. Rivero, C. Lopez, K. Richardson, A. Pope, A. Schulte, S. Myneni, H. Jain, K. Antoine and A. C. Miller, *J. Appl. Phys.*, 2005, **98**, 053503.
11 J. A. Freitas, U. Strom and D. J. Treacy, *J. Non-Cryst. Solids*, 1983, **59–60**, 875.
12 A. C. Wright, B. G. Aitken, G. Cuello, R. Haworth, R. N. Sinclair, J. R. Stewart and J. W. Taylor, *J. Non-Cryst. Solids*, 2011, **357**, 2502.
13 E. Bychkov, M. Miloshova, D. L. Price, C. J. Benmore and A. Lorriaux, *J. Non-Cryst. Solids*, 2006, **352**, 63.
14 E. Bychkov, C. J. Benmore and D. L. Price, *Phys. Rev. B: Condens. Matter Mater. Phys.*, 2005, **72**, 172107.
15 A. C. Wright, *J. Non-Cryst. Solids*, 1989, **112**, 33.
16 E. Lorch, *J. Phys. C: Solid State Phys.*, 1969, **2**, 229.
17 N. Norman, *Acta Crystallogr.*, 1957, **10**, 370.
18 J. Krogh-Moe, *Acta Crystallogr.*, 1956, **9**, 951.
19 A. L. Patterson, *Z. Kristallogr.*, 1935, **90**, 517.
20 A. K. Soper, *J. Phys.: Condens. Matter*, 2007, **19**, 335206.
21 M. Sheikbahae, A. A. Said, T. H. Wei, Y. Y. Wu, D. J. Hagan, M. J. Soileau and E. W. Vanstryland, *Z-Scan – A simple and sensitive technique for non-linear refraction measurements*, Spie - Int Soc Optical Engineering, Bellingham, 1990.
22 J. McCarthy, PhD thesis, Institute of Photonics and Quantum Sciences, Heriot-Watt University, 2013.
23 A. C. Hannon, *Nucl. Instrum. Methods Phys. Res., Sect. A*, 2005, **551**, 88.
24 A. K. Soper, Rutherford Appleton Laboratory Technical Report, RAL-TR-2011-013, 2011.
25 A. C. Hannon, W. S. Howells and A. K. Soper, *IOP Conf. Ser.*, 1990, **107**, 193.
26 A. P. Hammersley, ESRF Internal Report, ESRF98HA01T, 1998.
27 A. P. Hammersley, S. O. Svensson, M. Hanfland, A. N. Fitch and D. Hausermann, *High Pressure Res.*, 1996, **14**, 235.
28 L. B. Skinner, C. J. Benmore and J. B. Parise, *Nucl. Instrum. Methods Phys. Res., Sect. A*, 2012, **662**, 61.
29 A. K. Soper and E. R. Barney, *J. Appl. Crystallogr.*, 2011, **44**, 714.
30 N. E. Brese and M. O'Keeffe, *Acta Crystallogr., Sect. B: Struct. Sci.*, 1991, **47**, 192.
31 D. M. Pickup, R. Moss and R. J. Newport, *J. Appl. Crystallogr.*, 2014, **47**, 1790.
32 T. Wang, X. Gai, W. H. Wei, R. P. Wang, Z. Y. Yang, X. Shen, S. Madden and B. Luther-Davies, *Opt. Mater. Express*, 2014, **4**, 1011.
33 A. C. Stergiou and P. J. Rentzeperis, *Z. Kristallogr.*, 1985, **173**, 185.
34 R. J. Gillespie, *Chem. Soc. Rev.*, 1992, **21**, 59.
35 N. S. Abdel-Moneim, PhD thesis, Faculty of Engineering, University of Nottingham, 2012.
36 R. Y. Golovchak, A. Kozdras, C. Gorecki and O. I. Shpotyuk, *J. Non-Cryst. Solids*, 2006, **352**, 4960.
37 A. Feltz, H. Aust and A. Blayer, *J. Non-Cryst. Solids*, 1983, **55**, 179.
38 MDL SciGlass-6.0. MDL Information Systems, San Leandro, 2003.
39 I. Petri, P. S. Salmon and H. E. Fischer, *Phys. Rev. Lett.*, 2000, **84**, 2413.
40 D. G. Georgiev, P. Boolchand and K. A. Jackson, *Philos. Mag.*, 2003, **83**, 2941.
41 T. Wagner, S. O. Kasap, M. Vlček, A. Sklenar and A. Stronski, *J. Mater. Sci.*, 1998, **33**, 5581.
42 C. Y. Yang, M. A. Paesler and D. E. Sayers, *Phys. Rev. B: Condens. Matter Mater. Phys.*, 1989, **39**, 10342.
43 E. R. Barney, A. C. Hannon, D. Holland, D. Winslow, B. Rijal, M. Affatigato and S. A. Feller, *J. Non-Cryst. Solids*, 2007, **353**, 1741.
44 R. G. Orman, D. Holland and A. C. Hannon, *Phys. Chem. Glasses: Eur. J. Glass Sci. Technol., Part B*, 2008, **49**, 15.
45 G. Delaizir, M. Dussauze, V. Nazabal, P. Lecante, M. Dollé, P. Rozier, E. I. Kamitsos, P. Jovari and B. Bureau, *J. Alloys Compd.*, 2011, **509**, 831.
46 M. Deschamps, C. Roiland, B. Bureau, G. Yang, L. Le Pollès and D. Massiot, *Solid State Nucl. Magn. Reson.*, 2012, **40**, 72.
47 A. C. Hannon, Rutherford Appleton Laboratory Report, RAL-93-063, 1993.
48 B. Cordero, V. Gómez, A. E. Platero-Prats, R. Revés, J. Echeverría, E. Cremades, F. Barragán and S. Alvarez, *Dalton Trans.*, 2008, 2832.
49 J. S. Sanghera, C. M. Florea, L. B. Shaw, P. Pureza, V. Q. Nguyen, M. Bashkansky, Z. Dutton and I. D. Aggarwal, *J. Non-Cryst. Solids*, 2008, **354**, 462.

50 H. Nasu, K. Kubodera, M. Kobayashi, M. Nakamura and K. Kamiya, *J. Am. Ceram. Soc.*, 1990, **73**, 1794.
51 L. Petit, N. Carlie, A. Humeau, G. Boudebs, H. Jain, A. C. Miller and K. Richardson, *Mater. Res. Bull.*, 2007, **42**, 2107.
52 B. Jeansannetas, S. Blanchandin, P. Thomas, P. Marchet, J. C. Champarnaud-Mesjard, T. Merle-Mejean, B. Frit, V. Nazabal, E. Fargin, G. Le Flem, M. O. Martin, B. Bousquet, L. Canioni, S. Le Boiteux, P. Segonds and L. Sarger, *J. Solid State Chem.*, 1999, **146**, 329.
53 J. M. Harbold, F. O. Ilday, F. W. Wise and B. G. Aitken, *IEEE Photonics Technol. Lett.*, 2002, **14**, 822.
54 M. S. Maklad, R. K. Mohr, R. E. Howard, P. B. Macedo and C. T. Moynihan, *Solid State Commun.*, 1974, **15**, 855.
55 A. C. Hannon, *Neutron diffraction database*, http://www.alexhannon.co.uk/DBindex.htm, last accessed: [29/01/2015].